MSIRV Simulation for Dengue with Vaccination in a Complex Urban Domain

Amanda Maria Cardoso Cabral, Edivaldo Junior

https://doi.org/10.1590/SciELOPreprints.15069

Submitted on: 2026-02-09
Posted on: 2026-02-10 (version 1)
(YYYY-MM-DD)

PREPRINT VERSION – SUBMITTED FOR PUBLICATION

MSIRV Simulation for Dengue with Vaccination in a Complex Urban Domain

Amanda Maria Cardoso Cabral* [a]
amandamaria@ufrrj.br; https://orcid.org/0009-0009-5393-0483

Edivaldo Figueiredo Fontes Junior [b]
https://orcid.org/0000-0001-7555-345X

[a,b] Universidade Federal Rural do Rio de Janeiro (UFRRJ), Brazil

Abstract

This research investigates the spatiotemporal dynamics of dengue propagation using an MSIRV (Mosquito-Susceptible-Infected-Recovered-Vaccinated) epidemiological model. The central focus is the application of numerical methods (Finite Element Method, Crank-Nicolson Method, and Newton Method) to the model in real scenarios, integrating vaccination dynamics as a control parameter. The structure of the MSIRV model consists of a system of nonlinear partial differential equations. The computational implementation of the methods is verified using the Manufactured Solutions Method, which analyzes spatial convergence rates before their applicability to dynamic scenarios. The continuous spatial domain corresponds to the municipality of Seropédica (RJ). The simulations demonstrate that including the vaccination component significantly alters the viral infection rate. The model proved to be an effective prognostic tool for intervention planning and epidemic control. This research was conducted with the support of the Fundação de Amparo à Pesquisa do Estado do Rio de Janeiro - FAPERJ.

Keywords: Dengue, numerical methods, MSIRV.

1 Introduction

Mathematical models have become an essential and strategic tool for studying and analyzing the behavior of biological phenomena and systems of communicable diseases in human populations. In the case of arboviruses, such as dengue fever, models formulated as systems of partial differential equations allow us to predict the spatiotemporal propagation of infection across heterogeneous locations or to describe the current state of an epidemic. According to Yang (2001), the need to understand and predict disease behavior has given rise to a new field of science: mathematical epidemiology[2, 3].

Nonlinear systems of equations describe the interactions among the transmitter and infected, susceptible, and recovered individuals. In addition to the possibility of manipulating or extending the system to consider extra factors, such as rainfall, temperature, and vaccination control rates.

Varying the system to include parameters and equations that represent combat and control strategies is essential for public health. As Bassanezi (2002)[4] states, mathematical modeling is "the art of transforming real-world problems into mathematical problems and solving them by interpreting their solutions in the language of the real world."

The MSIRV model is based on the robust structure of the MSIR model formulated by Gomes (2009)[5], which demonstrates effectiveness in studying the dynamics of dengue propagation in his dissertation entitled "A Study on the Spread of Dengue Using Partial Differential Equations and Fuzzy Logic." The MSIRV model is an extension of the formulation consolidated by Gomes (2009), consisting of five nonlinear partial differential equations of the reaction-diffusion type, which represent the compartments of transmitting mosquitoes M, individuals susceptible to dengue S, individuals infected with dengue I, recovered individuals R, and vaccinated individuals V. The adaptation aims to document the impact of the vaccine during a dengue epidemic in the summer season, within an irregular boundary domain representing the municipality of Seropédica, Rio de Janeiro.

The nonlinear model includes diffusion terms that characterize the spatial-temporal displacement of vectors and individuals, and reaction terms that represent interactions between hosts and vectors. Finding an exact analytical solution to the model in real-world, dynamic scenarios is infeasible because it involves biological phenomena and requires accurate computational methods that preserve physical and biological conditions.

The numerical implementation proposed in this study is based on the Finite Element Method cite hughes for spatial discretization of the domain, owing to its ability to handle complex geometries. In addition to the Crank-Nicolson Method[7], which is a second-order method that offers unconditional stability, and the Newton Method[9], which linearizes the system and advances it in time.

Numerical verification of the methods applied to any computational model is essential when performing simulations in practical scenarios, in order to analyze the degree of convergence, determine the appropriate spatial and temporal discretization parameters, and analyze the accuracy of the methods[10] for the selected domain and period. To verify the methods, the Manufactured Solutions Method[11] is applied, and the expected decay of the numerical error is recorded as the mesh is refined.

Finally, the model is simulated, incorporating geographic data from IBGE [12] within the municipal domain of Seropédica (RJ), using the biologically validated parameters from the analytical study by Gomes (2009). The MSIRV model simulation transforms numerical analysis into a practical tool for health management.

The coupling of geographic data from Seropédica allows the simulation to reflect the environmental conditions that favor the proliferation of Aedes aegypti in the municipality. The objective of this article is to verify the numerical stability of the MSIRV model with computational numerical methods in an epidemic situation and to present the effectiveness of dengue dynamics under the effect of vaccination[25].

This research, in Section 2, presents the extension of the MSIR spatiotemporal model to the MSIRV model for the municipality of Seropédica, incorporating vaccination dynamics. Section 3 describes the numerical methodology, including the Finite Element Method, the Crank-Nicolson Method, and the Newton Method, and presents model verification using the Manufactured Solutions Method. Section 4 presents a study on the spatial domain used for the simulation. Section 5 discusses the results of the computational simulations, followed by the conclusion in Section 7.

The research is based on the robust MSIR (Mosquito - Susceptible - Infected - Recovered) compartmental structure developed by Gomes (2009)[5] to model vaccination dynamics in Seropédica. The model is a natural extension of the SIR (Susceptible - Infected - Recovered) model[13], established by epidemiologists William Ogilvy Kermack and Anderson Gray McKendrick in 1927, and expressed by equations (1)-(3).

$$\frac{\partial S}{\partial t} = -\beta SI; \tag{1}$$
$$\frac{\partial I}{\partial t} = \beta SI - \sigma I; \tag{2}$$
$$\frac{\partial R}{\partial t} = \sigma I \tag{3}$$

The transition dynamics between the compartments S, I, R is governed by the products βSI and σI, which correspond to the rate of infection and recovery from the disease.

- **Spatial dynamics of the MSIR model**

The dengue propagation dynamics of the MSIR model, as established by Gomes (2009)[5], describe the interaction between the transmitting mosquitoes M and the human populations (susceptible S, infected I, and recovered R). The consolidated MSIR model by Gomes (2009) considers the spatial distribution of mosquitoes and individuals through diffusion terms, resulting in the system of nonlinear partial differential equations presented in (4)-(7). The domain Ω in this work represents the topology of the municipality of Seropédica, Rio de Janeiro.

Let $\Omega \subseteq \mathbb{R}^2$ be the spatial domain and $[0, T_s]$ the time interval of the simulation. The system is governed by the state functions $\mathbf{M}, \mathbf{S}, \mathbf{I}, \mathbf{R}$ defined in $\Omega \times [0, T_s]$. The function $\mathbf{M}(x, y, t)$ represents the density of transmitting vectors, while the human population is divided into densities of susceptible $\mathbf{S}(x, y, t)$, infected $\mathbf{I}(x, y, t)$, and recovered $\mathbf{R}(x, y, t)$ individuals.

$$\frac{\partial \mathbf{M}}{\partial t} - \nabla \cdot \alpha_{\mathbf{M}} \nabla \mathbf{M} = (\nu - \mu)\mathbf{M}\,, \qquad \text{for } (x, y) \in \Omega \text{ e } t \in (0, T_s]; \tag{4}$$
$$\frac{\partial \mathbf{S}}{\partial t} - \nabla \cdot \alpha_{\mathbf{H}} \nabla \mathbf{S} = -\beta \mathbf{MS}\,, \qquad \text{for } (x, y) \in \Omega \text{ e } t \in (0, T_s]; \tag{5}$$
$$\frac{\partial \mathbf{I}}{\partial t} - \nabla \cdot \alpha_{\mathbf{H}} \nabla \mathbf{I} = \beta \mathbf{MS} - \sigma \mathbf{I}\,, \qquad \text{for } (x, y) \in \Omega \text{ e } t \in (0, T_s]; \tag{6}$$
$$\frac{\partial \mathbf{R}}{\partial t} - \nabla \cdot \alpha_{\mathbf{H}} \nabla \mathbf{R} = \sigma \mathbf{I}\,, \qquad \text{for } (x, y) \in \Omega \text{ e } t \in (0, T_s]. \tag{7}$$

The mobility of mosquitoes and individuals is characterized by the diffusive terms $\nabla \cdot \alpha_{\mathbf{M}} \nabla \mathbf{M}$ and $\nabla \cdot \alpha_{\mathbf{H}} \nabla$. In biological terms, the parameters ν and μ represent, respectively, the birth rate and the decay of the mosquito population. The evolution of the disease depends on the transmission parameter β and the recovery parameter σ.

- **Extension with vaccination control**

In this step, the model is expanded, preserving the original formulation by Gomes (2009)[5, 8], to incorporate intervention strategies. The state function $\mathbf{V}(x, y, t)$ was inserted to characterize the density of vaccinated individuals. The transition from susceptible to vaccinated individuals is governed by the temporal control parameter $\lambda(t)$.

In the partial differential equations (8)-(12) of the MSIRV model, it is considered that the vaccine reduces the susceptible population, so that it still has the possibility of being infected, but not severely enough to transition to the infected compartment $\mathbf{I}$.

$$\frac{\partial \mathbf{M}}{\partial t} - \nabla \cdot \alpha_{\mathbf{M}} \nabla \mathbf{M} = (\nu - \mu)\mathbf{M}\,, \qquad \text{for } (x,y) \in \Omega \text{ e } t \in (0, T_s]; \tag{8}$$

$$\frac{\partial \mathbf{S}}{\partial t} - \nabla \cdot \alpha_{\mathbf{H}} \nabla \mathbf{S} = -\beta \mathbf{M}\mathbf{S} - \lambda(t)\mathbf{S}\,, \qquad \text{for } (x,y) \in \Omega \text{ e } t \in (0, T_s]; \tag{9}$$

$$\frac{\partial \mathbf{I}}{\partial t} - \nabla \cdot \alpha_{\mathbf{H}} \nabla \mathbf{I} = \beta \mathbf{M}\mathbf{S} - \sigma \mathbf{I}\,, \qquad \text{for } (x,y) \in \Omega \text{ e } t \in (0, T_s]; \tag{10}$$

$$\frac{\partial \mathbf{R}}{\partial t} - \nabla \cdot \alpha_{\mathbf{H}} \nabla \mathbf{R} = \sigma \mathbf{I}\,, \qquad \text{for } (x,y) \in \Omega \text{ e } t \in (0, T_s]; \tag{11}$$

$$\frac{\partial \mathbf{V}}{\partial t} - \nabla \cdot \alpha_{\mathbf{H}} \nabla \mathbf{V} = \lambda(t)\mathbf{S}\,, \qquad \text{for } (x,y) \in \Omega \text{ e } t \in (0, T_s]; \tag{12}$$

According to records from the state health department[14], the municipality of Seropédica began vaccination in February 2024. This data, modeled by the parameter $\lambda(t)$, which represents the vaccine control rate, is set to a nonzero constant from the start of the official calendar in February 2024.

One property of the MSIRV model is the conservation of mass in the system. This property is characterized by Neumann boundary conditions across the entire boundary of the domain Ω. Thus, the MSIRV model considers the municipality of Seropédica to be an isolated system, where the variation and flow of M, S, I, R, V occur only internally.

The numerical methods used to solve the nonlinear system of equations are the Finite Element Method for spatial discretization, the Crank-Nicolson Method for temporal approximation, and the Newton Method for linearization and calculation of the solution of the resulting discretized system.

2 Methodology

This chapter presents the spatial and temporal discretization process using the Finite Element Method and the Crank-Nicolson Method, respectively, as well as the method used to linearize the system of partial differential equations. The numerical implementation is briefly verified using the MSIR model core to assess the convergence of the methods for the Seropédica grid. This verification ensures stability of the MSIRV model, since it is an extension of the dynamics of the original MSIR system.

- **Finite Element Method**

Let the test function space be $\mathbf{v_n} \in W^{k,p}(\Omega)$, called the Sobolev space over the domain Ω of the municipality of Seropédica. According to Adams and Fournier[15], the Sobolev space is a vector space whose elements are functions defined on an open domain in Euclidean $\mathbb{R}^n$, whose partial derivatives satisfy specific integrability conditions[16].

According to Damian and Nascimento[17]:

> The Sobolev space $W^{k,p}(\Omega)$ covers all functions $\mathbf{u} : \Omega \longrightarrow \mathbb{R}$, where for each multi-index α with $|\alpha| \leq k$, $D^\alpha \mathbf{u}$ exists in the weak sense and belongs to $L^p(\Omega)$, and can be written as $W^{k,p}(\Omega) = \{\mathbf{u} \in L^p(\Omega) : D^\alpha \mathbf{u} \in L^p(\Omega) \text{ for all } |\alpha| \leq k\}$.

In this study, the state functions $\mathbf{M}, \mathbf{S}, \mathbf{I}, \mathbf{R}$ are denoted by functions $\mathbf{u} \in L^p(\Omega)$, ensuring that the integration of the densities of M, S, I, R over the domain Ω results in

finite values, satisfying the Sobolev conditions necessary for the convergence of numerical methods.

The notation $L^p(\Omega)$ is defined by the Lebesgue space and $D^\alpha \mathbf{u}$ are partial derivatives of $\mathbf{u}$, where the multi-index a defines the order of this partial derivative. The spatial domain $\Omega \subset \mathbf{R}^2$ represents the limited region of the municipality of Seropédica.

The weak form, or variational form, is obtained by applying the Divergence Theorem to the MSIRV system equations, which allows the order of the derivatives of the diffusion terms $\nabla \cdot \alpha \nabla$ to be reduced, and by multiplying this system of equations by test functions $\mathbf{v_n}$, which allow partial differential equations to be converted into integrals belonging to the space $W^{1,2}(\Omega)$, where $k = 1$ guarantees the existence of first-order derivatives in the weak sense and $p = 2$ guarantees the existence of the inner product.

In the weak formulation, the terms $\mathbf{M_g}, \mathbf{S_g}, \mathbf{I_g}, \mathbf{R_g}$ represent the global solutions for the entire spatial mesh, calculated iteratively at each discrete time step. Integrating the equations over the domain Ω, we obtain the following weak forms (13)-(16) of the system:

$$\int_\Omega \frac{\partial \mathbf{M}_g}{\partial t} \cdot \mathbf{v}_n d\Omega + \int_\Omega (\alpha_M \nabla \mathbf{M}_g) \cdot (\nabla \mathbf{v}_n) d\Omega - \int_\Omega (\nu \mathbf{M}_g - \mu \mathbf{M}_g + f_0) \mathbf{v}_n d\Omega = 0 \tag{13}$$

$$\int_\Omega \frac{\partial \mathbf{S}_g}{\partial t} \cdot \mathbf{v}_n d\Omega + \int_\Omega (\alpha_H \nabla \mathbf{S}_g) \cdot (\nabla \mathbf{v}_n) d\Omega + \int_\Omega \beta \mathbf{M}_g \mathbf{S}_g \cdot \mathbf{v}_n d\Omega - \int_\Omega f_1 \cdot \mathbf{v}_n d\Omega = 0 \tag{14}$$

$$\int_\Omega \frac{\partial \mathbf{I}_g}{\partial t} \cdot \mathbf{v}_n d\Omega + \int_\Omega (\alpha_H \nabla \mathbf{I}_g) \cdot (\nabla \mathbf{v}_n) d\Omega - \int_\Omega (\beta \mathbf{M}_g \mathbf{S}_g - \sigma \mathbf{I}_g) \cdot \mathbf{v}_n d\Omega - \int_\Omega f_2 \cdot \mathbf{v}_n d\Omega = 0 \tag{15}$$

$$\int_\Omega \frac{\partial \mathbf{R}_g}{\partial t} \cdot \mathbf{v}_n d\Omega + \int_\Omega (\alpha_H \nabla \mathbf{R}_g) \cdot (\nabla \mathbf{v}_n) d\Omega - \int_\Omega (\sigma \mathbf{I}_g) \cdot \mathbf{v}_n d\Omega - \int_\Omega f_3 \cdot \mathbf{v}_n d\Omega = 0 \tag{16}$$

The discretization of the spatial domain Ω was performed using Gmsh software[18], generating a mesh (1) composed of triangular elements, representing the municipality of Seropédica. The mesh transforms the continuous domain into a union of simple subdomains.

In the Finite Element Method, the quality of spatial discretization is essential for the convergence of the method. Mesh refinement minimizes interpolation error among the state variables $\mathbf{M}, \mathbf{S}, \mathbf{I}, \mathbf{R}$, ensuring the necessary accuracy for computational simulations that incorporate biological parameters.

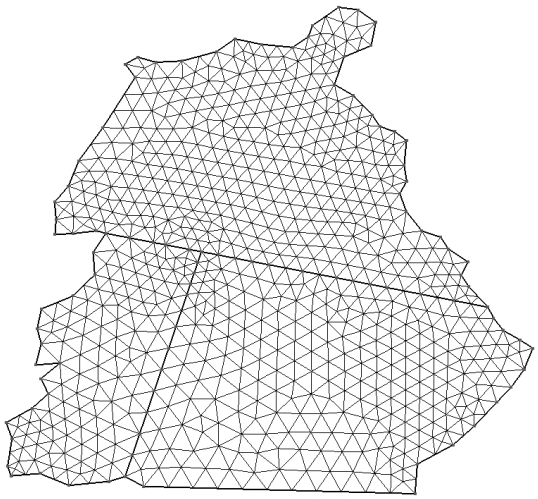

Figure 1: Discretized domain with 750 nodes and 1392 finite elements.

The next topic details the temporal discretization and the treatment of the system's nonlinear terms.

- **Crank-Nicolson method and system resolution**

For temporal discretization, the Crank-Nicolson method was adopted, a second-order implicit method with a single time step. The discretizations of the transient terms (17)-(20) are expressed by the difference centered at $t^{(n+1)/2}$, connecting the known solution at step t^n, starting from $t = 0$ (initial conditions), and the unknown at the next time step t^{n+1}.

$$\left.\frac{\partial \mathbf{M}_g}{\partial t}\right|_{[t^n,t^{n+1}]} \approx \underbrace{\frac{\mathbf{M}_g^{n+1}-\mathbf{M}_g^n}{\Delta t}}_{\text{Transient Term}} = \frac{1}{2}\left[F(\mathbf{M}_g^{n+1})+F(\mathbf{M}_g^n)\right] \qquad \text{(Mosquitoes)} \qquad (17)$$

$$\left.\frac{\partial \mathbf{S}_g}{\partial t}\right|_{[t^n,t^{n+1}]} \approx \underbrace{\frac{\mathbf{S}_g^{n+1}-\mathbf{S}_g^n}{\Delta t}}_{\text{Transient Term}} = \frac{1}{2}\left[F(\mathbf{S}_g^{n+1})+F(\mathbf{S}_g^n)\right] \qquad \text{(Susceptible)} \qquad (18)$$

$$\left.\frac{\partial \mathbf{I}_g}{\partial t}\right|_{[t^n,t^{n+1}]} \approx \underbrace{\frac{\mathbf{I}_g^{n+1}-\mathbf{I}_g^n}{\Delta t}}_{\text{Transient Term}} = \frac{1}{2}\left[F(\mathbf{I}_g^{n+1})+F(\mathbf{I}_g^n)\right] \qquad \text{(Infected)} \qquad (19)$$

$$\left.\frac{\partial \mathbf{R}_g}{\partial t}\right|_{[t^n,t^{n+1}]} \approx \underbrace{\frac{\mathbf{R}_g^{n+1}-\mathbf{R}_g^n}{\Delta t}}_{\text{Transient Term}} = \frac{1}{2}\left[F(\mathbf{R}_g^{n+1})+F(\mathbf{R}_g^n)\right] \qquad \text{(Recovered)} \qquad (20)$$

In this method, the operator $F(\Phi)$ represents the sum of the diffusion and reaction terms associated with the state variable Φ.

The infection term βMS represents a nonlinearity that prevents the direct solution of the MSIR model's system of algebraic equations. In this case, Newton's method was used to linearize the problem and solve it iteratively at each time step. The complete form, with spatial discretization and the Crank-Nicolson method applied, takes the form (21)-(24):

$$\begin{aligned}\int_\Omega \frac{\mathbf{M}_g^{n+1}}{\Delta t}\cdot\mathbf{v}_n d\Omega + \frac{1}{2}\int_\Omega (\alpha_M \nabla \mathbf{M}_g^{n+1})\cdot(\nabla \mathbf{v}_n)d\Omega - \frac{1}{2}\int_\Omega (\nu \mathbf{M}_g^{n+1} - \mu \mathbf{M}_g^{n+1})\cdot\mathbf{v}_n d\Omega \\ = \int_\Omega \frac{\mathbf{M}_g^{n}}{\Delta t}\cdot\mathbf{v}_n d\Omega \\ - \frac{1}{2}\int_\Omega (\alpha_M \nabla \mathbf{M}_g^{n})\cdot(\nabla \mathbf{v}_n)d\Omega + \frac{1}{2}\int_\Omega (\nu \mathbf{M}_g^{n} - \mu \mathbf{M}_g^{n})\cdot\mathbf{v}_n d\Omega \end{aligned} \tag{21}$$

$$\begin{aligned}\int_\Omega \frac{\mathbf{S}_g^{n+1}}{\Delta t}\cdot\mathbf{v}_n d\Omega + \frac{1}{2}\int_\Omega (\alpha_H \nabla \mathbf{S}_g^{n+1})\cdot(\nabla \mathbf{v}_n)d\Omega + \frac{1}{2}\int_\Omega \beta \mathbf{M}_g^{n+1}\mathbf{S}_g^{n+1}\cdot\mathbf{v}_n d\Omega \\ = \int_\Omega \frac{\mathbf{S}_g^{n}}{\Delta t}\cdot\mathbf{v}_n d\Omega \\ - \frac{1}{2}\int_\Omega (\alpha_H \nabla \mathbf{S}_g^{n})\cdot(\nabla \mathbf{v}_n)d\Omega - \frac{1}{2}\int_\Omega \beta \mathbf{M}_g^{n}\mathbf{S}_g^{n}\cdot\mathbf{v}_n d\Omega \end{aligned} \tag{22}$$

$$\begin{aligned}\int_\Omega \frac{\mathbf{I}_g^{n+1}}{\Delta t}\cdot\mathbf{v}_n d\Omega + \frac{1}{2}\int_\Omega (\alpha_H \nabla \mathbf{I}_g^{n+1})\cdot(\nabla \mathbf{v}_n)d\Omega + \frac{1}{2}\int_\Omega \sigma \mathbf{I}_g^{n+1}\cdot\mathbf{v}_n d\Omega \\ = \int_\Omega \frac{\mathbf{I}_g^{n}}{\Delta t}\cdot\mathbf{v}_n d\Omega \\ - \frac{1}{2}\int_\Omega (\alpha_H \nabla \mathbf{I}_g^{n})\cdot(\nabla \mathbf{v}_n)d\Omega - \frac{1}{2}\int_\Omega \sigma \mathbf{I}_g^{n}\cdot\mathbf{v}_n d\Omega \\ + \frac{1}{2}\int_\Omega \beta(\mathbf{M}_g^{n+1}\mathbf{S}_g^{n+1} + \mathbf{M}_g^{n}\mathbf{S}_g^{n})\cdot\mathbf{v}_n d\Omega \end{aligned} \tag{23}$$

$$\begin{aligned}\int_\Omega \frac{\mathbf{R}_g^{n+1}}{\Delta t}\cdot\mathbf{v}_n d\Omega + \frac{1}{2}\int_\Omega (\alpha_H \nabla \mathbf{R}_g^{n+1})\cdot(\nabla \mathbf{v}_n)d\Omega \\ = \int_\Omega \frac{\mathbf{R}_g^{n}}{\Delta t}\cdot\mathbf{v}_n d\Omega \\ - \frac{1}{2}\int_\Omega (\alpha_H \nabla \mathbf{R}_g^{n})\cdot(\nabla \mathbf{v}_n)d\Omega \\ + \frac{1}{2}\int_\Omega \sigma(\mathbf{I}_g^{n+1} + \mathbf{I}_g^{n})\cdot\mathbf{v}_n d\Omega \end{aligned} \tag{24}$$

This system can be represented in a compact form by a global residual vector $\mathbf{R}_g(\mathbf{u}^{n+1})$ that represents the deviation of the solution, at a given time step, from the equilibrium of the discretized equations. Since the term $\beta\mathbf{M_g}\mathbf{S_g}$ is nonlinear in the equations for susceptible individuals and infected individuals, Newton's method is applied.

The Newton method solves the system iteratively using the Jacobian matrix $\mathbf{J}$, present in (25), whose elements are the partial derivatives of each of the five global residuals, exposed in equations (21)- (24), in relation to each variable of the solution vector

$\mathbf{u} = [\mathbf{M_g}, \mathbf{S_g}, \mathbf{I_g}, \mathbf{R_g}]^T$.

$$\mathbf{J} = \begin{bmatrix} \frac{\partial R_M}{\partial \mathbf{M}_g} & \frac{\partial R_M}{\partial \mathbf{S}_g} & \frac{\partial R_M}{\partial \mathbf{I}_g} & \frac{\partial R_M}{\partial \mathbf{R}_g} \\ \frac{\partial R_S}{\partial \mathbf{M}_g} & \frac{\partial R_S}{\partial \mathbf{S}_g} & \frac{\partial R_S}{\partial \mathbf{I}_g} & \frac{\partial R_S}{\partial \mathbf{R}_g} \\ \frac{\partial R_I}{\partial \mathbf{M}_g} & \frac{\partial R_I}{\partial \mathbf{S}_g} & \frac{\partial R_I}{\partial \mathbf{I}_g} & \frac{\partial R_I}{\partial \mathbf{R}_g} \\ \frac{\partial R_R}{\partial \mathbf{M}_g} & \frac{\partial R_R}{\partial \mathbf{S}_g} & \frac{\partial R_R}{\partial \mathbf{I}_g} & \frac{\partial R_R}{\partial \mathbf{R}_g} \end{bmatrix} \tag{25}$$

In the matrix structure, each element $J_{i,j} = \frac{\partial R_i}{\partial \mathbf{u}_j}$ describes the influence of compartment j on the equation of compartment i. That is, the Jacobian matrix must organize biological interactions (linked to reaction terms) and spatial interactions (linked to diffusion terms) into a single structure, thereby enabling Newton's method to linearize and solve the system iteratively at each fixed time step, with $\Delta t = 0.5$ in Crank-Nicolson's method.

In Newton's method, at each iteration k, a correction $\Delta \mathbf{u}^k$ is calculated for the solution through the system (26):

$$\mathbf{J}(\mathbf{u}^{n+1,k})\Delta \mathbf{u}^k = -\mathbf{R}_g(\mathbf{u}^{n+1,k}) \tag{26}$$

This correction step $\Delta \mathbf{u}^k$ has the function of adjusting the solution of all compartments simultaneously so that accuracy is achieved, until a tolerance (stop criterion) defined at 10^{-8} is reached.

To verify the numerical implementation with the spatial mesh of the municipality of Seropédica, a spatial convergence analysis was performed using the Manufactured Solutions Method[26], in which an exact solution $\mathbf{u_g}(x, y, t) = (1 + t)(x^2 + y^2)$ and the error norm between the computational solution obtained and the analytical solution was calculated for different mesh refinements.

The discretization errors were analyzed for three different refinements[28], setting $\Delta t = 0.05$. The initial mesh consists of 750 nodes and 1392 finite elements. The first refinement, based on this mesh, resulted in 2891 nodes and 5568 finite elements. The second refinement obtained 11,349 nodes and 22,400 elements. According to table 1, the numerical verification demonstrated convergence of the computational solution for the applied methods, which confirms the consistency of the structure and the correct implementation of the model.

Table 1: Spatial convergence analysis for the computational solution.

Refinement	**Nodes**	**Elements**	**Global error**
Original mesh	750	1392	1.5546×10^{-4}
Refinement 1	2891	5568	3.6295×10^{-5}
Refinement 2	11349	22272	8.8209×10^{-6}

It can be observed that, by quadrupling the number of finite elements in the mesh, the global error is reduced by a factor of 4, reaching the order of 10^{-6} for the third refinement. The graph shows the behavior of the global error norm relative to the theoretical reference line, which has a slope of 2, as expected for the second-order Crank-Nicolson method. In this graph, the error curve appears to be approximately parallel to the reference line. This factor confirms the convergence of the methods and the model's correct implementation.

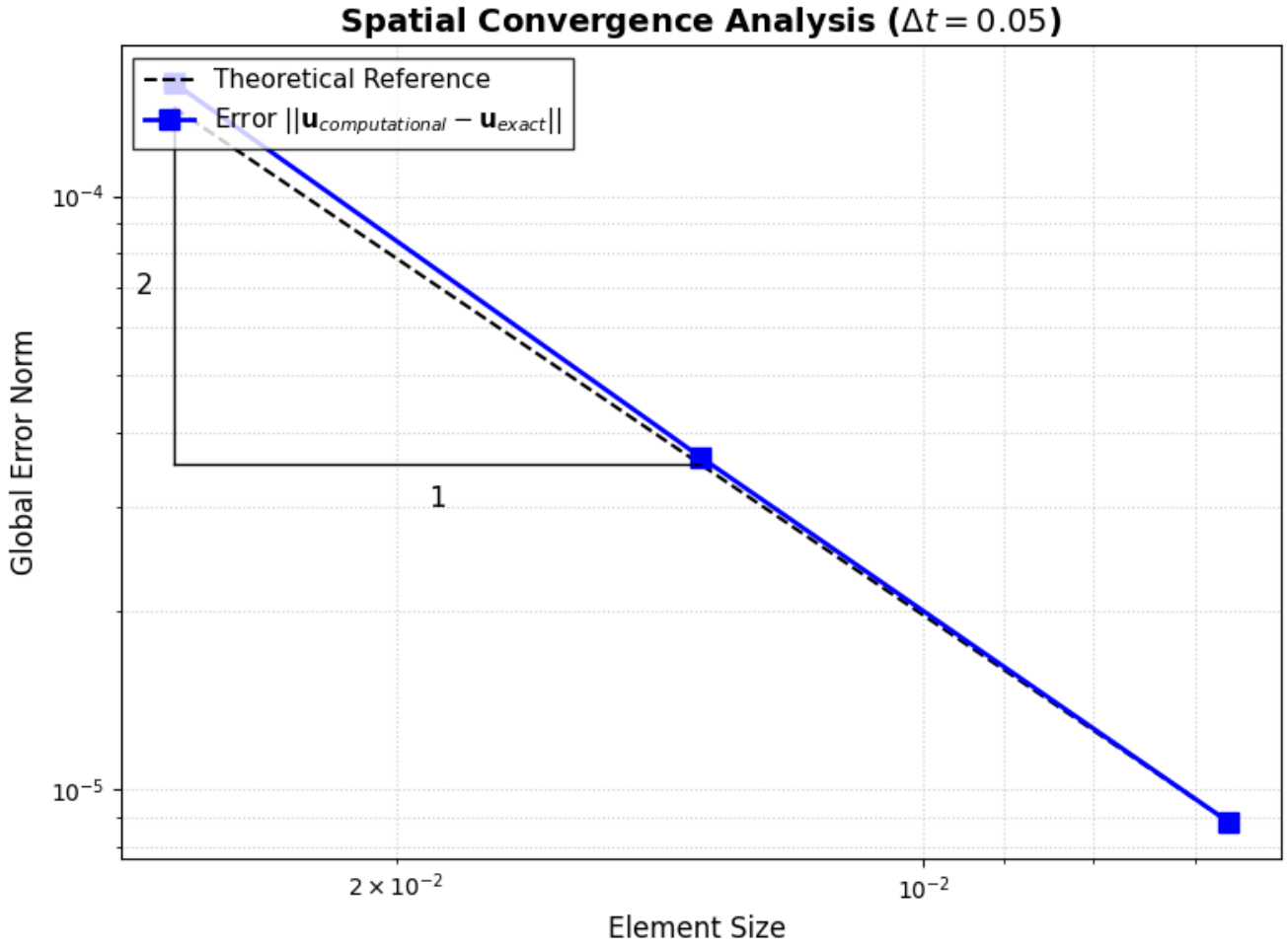

Figure 2: Straight line reference and global error

After verifying the computational implementation of the methods coupled to the MSIR model, the next section examines the spatial domain and performs a simulation with realistic parameters using the MSIRV model. This step defines system conditions and parameters, taking into account geographic and climatic data, individual and mosquito densities, and vaccination dynamics.

3 Domain study and parameter formulation

For the study of domain Ω, while the classic SIR model uses a homogeneous population, the MSIRV model considers spatial heterogeneity by dividing the municipality of Seropédica into three distinct regions.

The heterogeneity in this study is represented by the demarcation of the municipality into three distinct regions (red, orange, and yellow), as shown in figure (3), in which each region has a geographical characteristic, as represented in table 2:

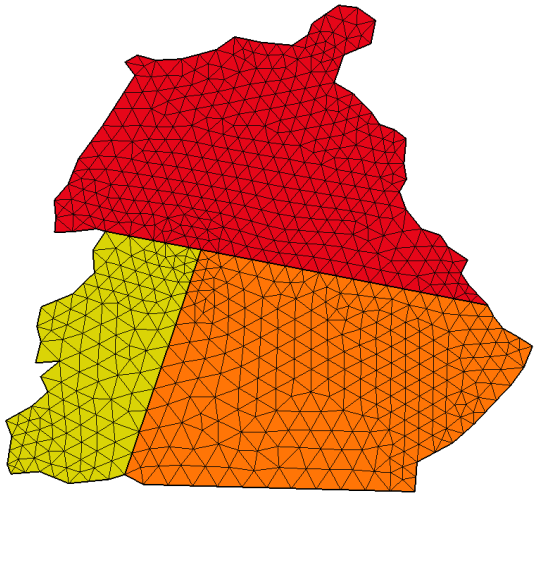

Figure 3: Demarcation of domain Ω (municipality of Seropédica, RJ) into three distinct regions.

The model's determinations of geographic areas and population distribution were based on inferential analysis, given the scarcity of detailed official information at the neighborhood level. Therefore, the values were based on territorial landmarks and data from the Brazilian Institute of Geography and Statistics (IBGE)[12].

Region 1 was delimited by the Campo Lindo neighborhood, which covers approximately 14.4 km² and has 15,573 inhabitants[12], and by the area occupied by the Federal Rural University of Rio de Janeiro, which covers approximately 30.24 km²[19]. Thus, the total area of this region was set at approximately 45 km².

For region 2, the Areeiro District of Piranema was considered, with an average area of 50 km²[20], the Canto do Rio neighborhood, with approximately 0.5 km², based on the donation of 50 hectares by INCRA[21], and Fazenda Caxias, which has plots of varying sizes (between 214 m^2 and 4,050 m^2). Therefore, the total area of region 2 was calculated to be approximately 100 km^2.

Region 3 was defined as 120.3 km²; this value was established as a geographical residue in order to complete the total area of the municipality of Seropédica, which is equivalent to 265,289 km². Population distribution estimates for the year 2024 were made similarly for each region:

Table 2: Area and estimated population by region for the municipality of Seropédica.

Region	**Area (km^2)**	**Population**	**Density ($N°$/km^2)**
Region 1 (yellow)	45.0	20,000	444.4
Region 2 (orange)	100.0	30,000	300
Region 3 (red)	120.3	38,000	315.88

To define the simulation period, the months from December 2023 to March 2024 were analyzed using meteorological data from INMET (National Institute of Meteorology) [22].

High rainfall during this period is a major environmental factor contributing to the onset of a dengue epidemic. High rainfall can cause water to accumulate in containers, depressions in the ground, and gutters, creating ideal breeding grounds for mosquitoes. The temperatures and rainfall recorded by the National Institute of Meteorology were adapted in figure (4) for the municipality of Seropédica.

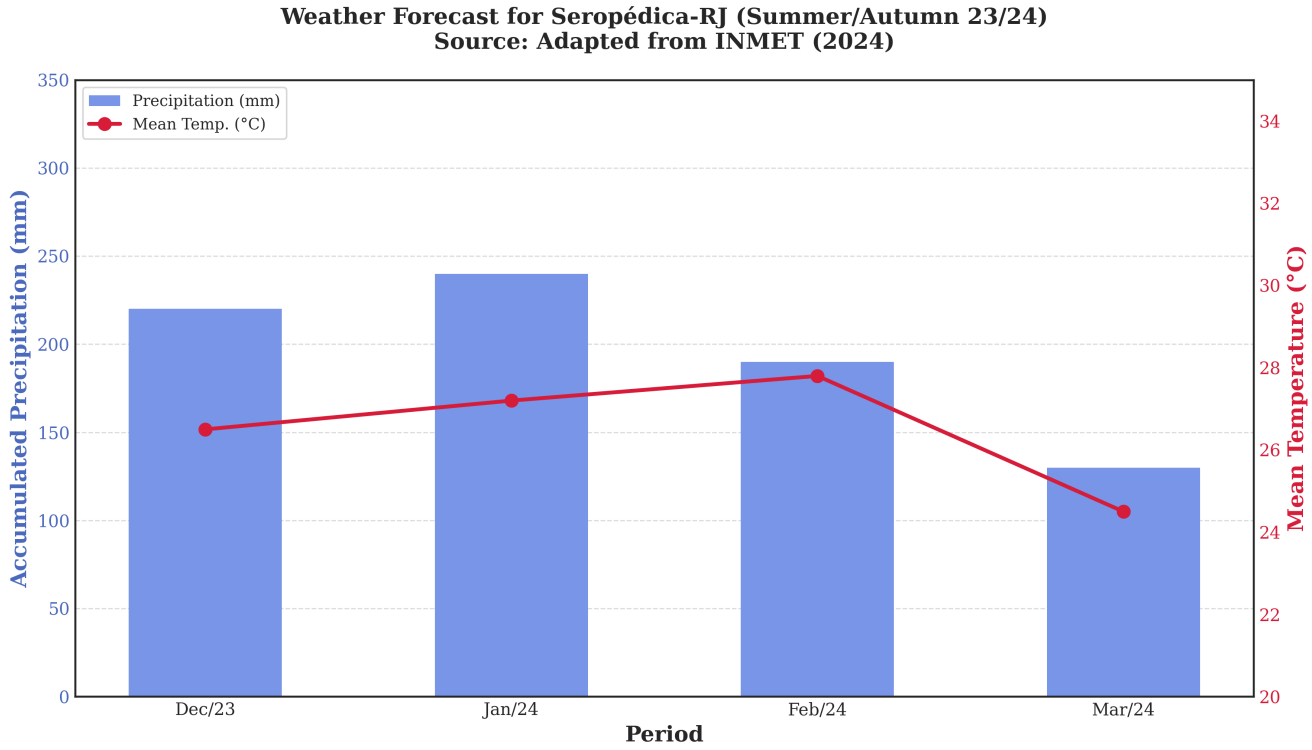

Figure 4: Precipitation and average temperature forecast by INMET for the summer quarter.

Information on climate trends enables connections between model variables and local phenomena, such as vector proliferation and its impact on disease spread. The choice of the simulation period is reflected in the observation that dengue transmission is exacerbated in the summer, thereby increasing the incidence of reported cases. In this context, public health interventions are essential, including vaccination as a control measure.

According to the Ministry of Health [23], vaccination was administered on February 23, 2024, in the municipality, with approximately 2,159 doses. Thus, the parameter that indicates the vaccination rate $\lambda(t)$ of the municipality can be expressed as a function of simulation time t:

$$\lambda(t) \approx \begin{cases} 0.00064/\text{day}, & \text{if } t \geq 23/02/2024 \\ 0, & \text{if} t < 23/02/2024 \end{cases} \tag{27}$$

In the spatial propagation model of dengue fever, the evolution and distribution of the disease are simulated using initial and boundary conditions. For the vector compartments M, susceptible individuals S, infected individuals I, recovered individuals R, and vaccinated individuals V, the initial conditions are the state of the system at time $t = 0$.

To ensure the biological consistency of the model, this study adapts the reference parameters consolidated in the methodology of Gomes (2009)[5] for the municipality of Seropédica. Therefore, the initial density of infected individuals was set at 0.005 inhabitants/km^2 and the initial density of vectors at 300 vectors/km^2, aiming to represent the initial stage of an epidemic. According to the methodology of Gomes (2009), the initial condition for susceptible individuals was characterized by the population density of each region subtracted from the density of infected individuals, as in (28):

$$S(x, y, 0) = \text{Population density} - 0.005 \text{ inhabitants/km}^2 \tag{28}$$

The initial condition values for the simulation in Seropédica are presented in table 3, where the initial conditions for all individuals S, I, R, V respect the total population density ($N°/km^2$) for each region.

Table 3: Initial conditions for the MSIRV epidemiological model by region (Density).

Region	$M(0)$	$S(0)$	$I(0)$	$R(0)$	$V(0)$
Region 1	300	444.39	0.005	0	0
Region 2	300	299.99	0.005	0	0
Region 3	300	315.87	0.005	0	0

Table 4: Biological and dispersion parameters calibrated for the municipality of Seropédica, based on the analysis by Gomes (2009).

Parameter	**Definition**	**Value**
α_H	Human dispersion coefficient	$0.010\, km^2/day$
α_M	Mosquito dispersion coefficient	$0.0010\, km^2/day$
β	Dengue propagation speed	$0.00002/day$
ν	Vector birth rate	$0.04/day$
μ	Vector mortality rate	$0.03/day$
σ	Recovery rate	$0.14/day$

$$\frac{\partial M}{\partial t} - \nabla \cdot \alpha_M \nabla M = \nu M - \mu M\,, \qquad \text{para } (x,y) \in \Omega \text{ e } t \in (0, T_s]; \tag{29}$$

$$\frac{\partial S}{\partial t} - \nabla \cdot \alpha_H \nabla S = -\beta M S - \lambda(t) S\,, \qquad \text{para } (x,y) \in \Omega \text{ e } t \in (0, T_s]; \tag{30}$$

$$\frac{\partial I}{\partial t} - \nabla \cdot \alpha_H \nabla I = \beta S M - \sigma I\,, \qquad \text{para } (x,y) \in \Omega \text{ e } t \in (0, T_s]; \tag{31}$$

$$\frac{\partial R}{\partial t} - \nabla \cdot \alpha_H \nabla R = \sigma I\,, \qquad \text{para } (x,y) \in \Omega \text{ e } t \in (0, T_s]; \tag{32}$$

$$\frac{\partial V}{\partial t} - \nabla \cdot \alpha_H \nabla V = \lambda(t) S\,, \qquad \text{para } (x,y) \in \Omega \text{ e } t \in (0, T_s]; \tag{33}$$

The adjustments calibrate the model to the municipality's local dynamics while preserving the canonical structure of the dispersion and transition terms established in the reference study, thereby ensuring simulation consistency.

4 Results

This section presents the results of the numerical simulation of the MSIRV model for the period from December 1, 2023, to March 31, 2024, totaling 122 days of projection. This interval encompasses the period of highest rainfall and temperature in the municipality of Seropédica.

The simulation graphs were generated using ParaView software[24], at the initial time $t = 0$, equivalent to December 1, 2023, until time $t = 122$, referring to the end of the simulation on March 31, 2024. For infected individuals, the epidemic peak occurs on January 28 ($t = 58$) in the simulation.

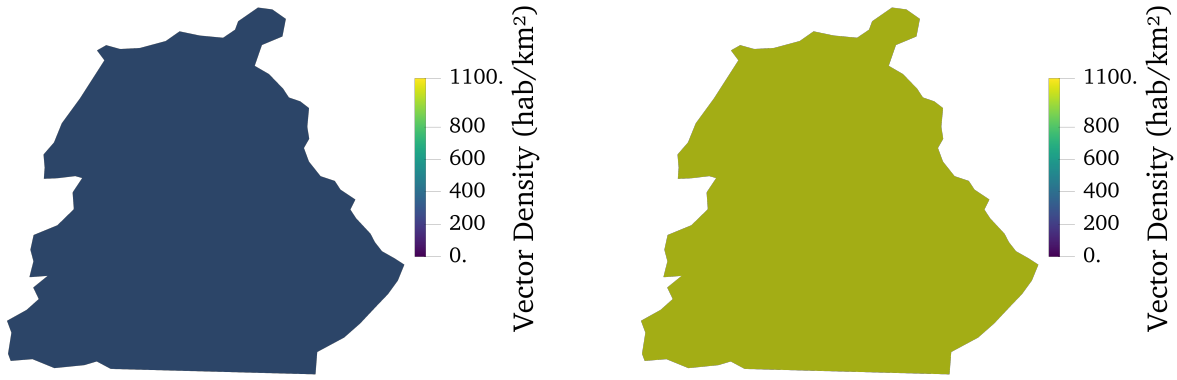

(a) Vector Density (hab/km^2) at $t = 0$.

(b) Vector Density (hab/km^2) at $t = 122$.

Figure 5: Mosquito density M throughout the simulation.

In figure (4), it is possible to observe the exponential growth of transmitting mosquitoes throughout the simulation. This growth is caused by birth rates ν that are higher than

mortality rates μ, which ensure that there are enough vectors to sustain the epidemic throughout the simulation time, even with a low infection rate β.

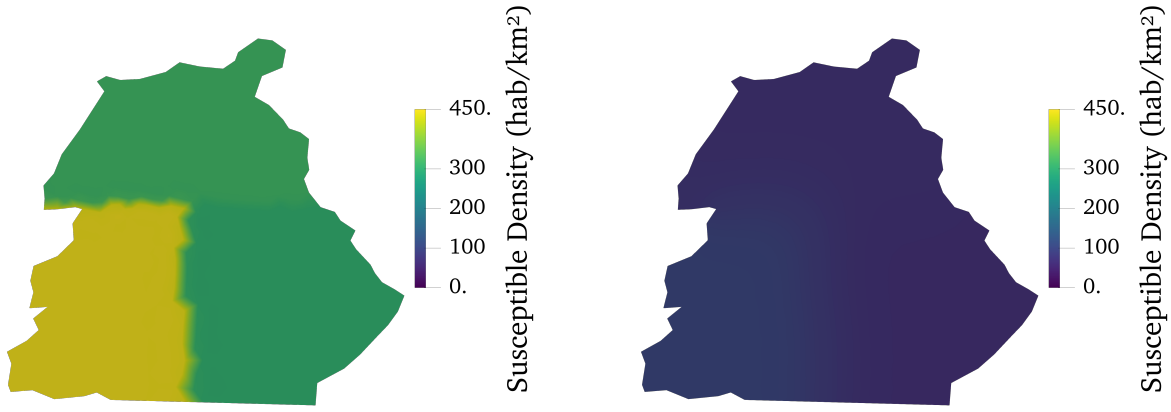

(a) Susceptible Density (hab/km^2) at $t = 0$.

(b) Susceptible Density (hab/km^2) at $t = 122$.

Figure 6: Density of susceptible individuals S throughout the simulation.

The graph (6(b)) shows, in its blue coloring in region 1, at the end of the simulation, that not all susceptible individuals were infected during this period. That is, dengue fever did not affect 100% of the local population, and there remain individuals who have not moved into the vaccinated compartment V. The purple color in this graph indicates that the individuals present in these regions were infected and have recovered.

(a) Infection Density (hab/km^2) at $t = 0$.

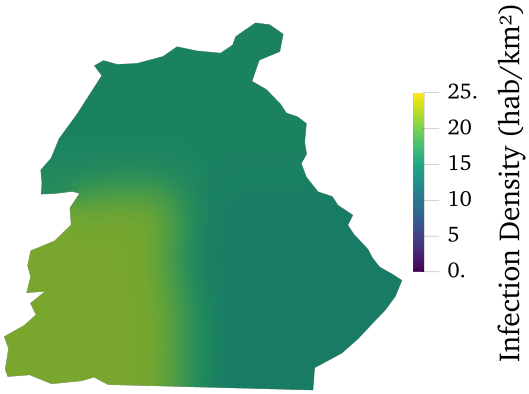

(b) Infection Density (hab/km^2) at $t = 62$.

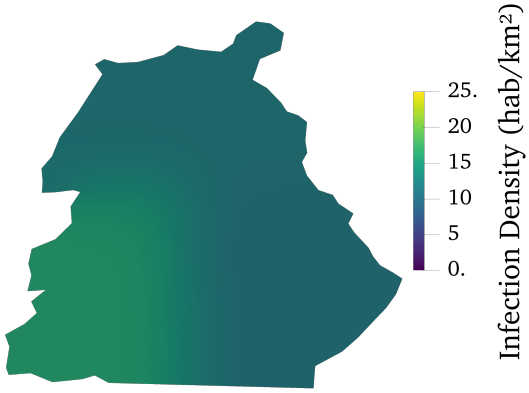

(c) Infection Density (hab/km^2) at $t = 122$.

Figure 7: Density of infected individuals I throughout the simulation.

For the compartment of infected individuals in figure (7), it can be observed that at $t = 0$ (December 1, 2023), the infection is not yet visible in the domain. At $t = 58$ (January 28, 2024), the highest number of infections occurs; in region 1, with the highest population density, the density of infected individuals reaches approximately 25 inhabitants per km^2.

In addition, the peak in infections precedes the start of vaccination in the municipality (February 23, 2024). figure (7(c)), at $t = 122$ (March 31, 2024), shows that the density of infected individuals reaches approximately 15 to 20 inhabitants per km^2 and does not reach zero completely, indicating that dengue remains active in the area and not all infected individuals have recovered or been vaccinated.

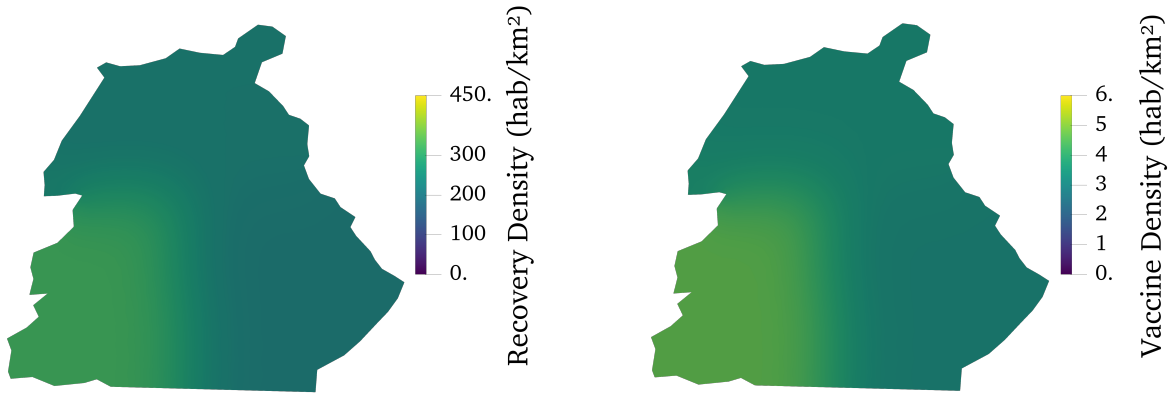

(a) Recovery Density (hab/km^2) at $t = 122$.

(b) Vaccine Density (hab/km^2) at $t = 122$.

Figure 8: Density of vaccinated individuals V throughout the simulation.

The density of vaccinated individuals at $t = 122$, in figure (8(b)), has values between 4 and 6 inhabitants per km^2 in the municipality. These values are consistent with the slow vaccination rate in the area ($\lambda(t) = 0.0008$), attributable to the limited number of doses distributed (2,159) and the relatively late start on February 23, 2024.

Therefore, the vaccine intervention was delayed, as it began after the infection peaked (January 28). In addition, the number of vaccine doses, given the municipality's population size and geographic area, was insufficient to effectively vaccinate the population and was effective only at the end of the simulation, when most individuals had already been infected.

The results obtained are essential for computational modeling. By simulating realistic scenarios, the model can generate epidemics without instability and highlights the need for early interventions, such as controlling mosquito proliferation, avoiding the accumulation of standing water, and administering vaccines early [1].

5 Conclusions

The research in this study demonstrated that the MSIRV model provides a consistent representation of the spatiotemporal dynamics of dengue, particularly when accounting for the influence of interventions.

The simulation graphs indicated that the inclusion of the vaccinated compartment V consistently represented the density of vaccinated individuals and the spatial rhythm of this compartment under the domain. The results reaffirm the structural effectiveness of the MSIR base model proposed by Gomes (2009)[5], which provides a fundamental and reliable framework for extending the presented vaccination dynamics. The simulation enabled analysis to extend beyond the theoretical level. Thus, it was possible to identify the locations with the highest population density and those requiring greater attention for combat and intervention measures within the municipality.

The Finite Element Method coupled with the Crank-Nicolson Method demonstrated

stability and spatial convergence, demonstrating the applicability of high-order methods to epidemiological problems involving domains with complex contours[27]. In addition, the Newton method handled the nonlinear components of the system, ensuring the necessary accuracy for interpreting biological data.

Verification using the Manufactured Solutions Method was essential for analyzing spatial convergence for the grid depicting the municipality. Through this method, the fluidity of the Crank-Nicolson Finite Element Method was observed, as evidenced by a reduction in overall error as refinement was applied, as required by numerical analysis.

Therefore, the simulation's success and its applicability to real-world scenarios encourage the continued use of computational models to combat epidemics in the target location.

DATA AVAILABILITY STATEMENT The concepts supporting the findings of this study were derived from the following public domains: IBGE, INMET, and the Municipal Health Secretariat. Additionally, specific modeling parameters were adapted from Gomes (2009). All data are available through their respective official institutional repositories.

CONFLICT OF INTEREST The authors declare that there is no conflict of interest regarding the publication of this manuscript.

AUTHOR CONTRIBUTIONS

- **Amanda Maria Cardoso Cabral:** Conceptualization · Data curation · Formal analysis · Investigation · Methodology · Validation · Visualization · Writing - original draft preparation · Writing - review & editing
- **Edivaldo Figueiredo Fontes Junior:** Funding acquisition · Project administration · Supervision

FUNDING This research was conducted with the support of the Fundação de Amparo à Pesquisa do Estado do Rio de Janeiro - FAPERJ.

References

[1] A. Wilder-Smith, Dengue vaccination: the long road to implementation, The Lancet Infectious Diseases 24 (2024) 453-455.

[2] L.R. Alvarenga, Modelagem de epidemias através de modelos baseados em indivíduos, Dissertação (Mestrado), Universidade Federal de Minas Gerais, Belo Horizonte, 2008.

[3] H.M. Yang, Epidemiologia matemática: estudo dos efeitos da vacinação em doenças de transmissão direta, Editora da Unicamp, Campinas, 2001.

[4] R.C. Bassanezi, Ensino-aprendizagem com modelagem matemática: uma nova estratégia, Editora Contexto, São Paulo, 2002.

[5] L.T. Gomes, Um Estudo Sobre o Espalhamento da Dengue Usando Equações Diferenciais Parciais e Lógica Fuzzy, Master's Thesis, UNICAMP, Campinas, 2009.

[6] T.J.R. Hughes, The Finite Element Method: Linear Static and Dynamic Finite Element Analysis, Dover Publications, Mineola, 2000.

[7] A. Quarteroni, R. Sacco, F. Saleri, Numerical Mathematics, second ed., Springer-Verlag, Berlin, 2007.

[8] L. Cattarino, et al., The spatial dynamics of dengue transmission: a review of modeling insights and challenges, Lancet Infect. Dis. 24 (2024) 112-125.

[9] R.L. Burden, J.D. Faires, Numerical Analysis, ninth ed., Cengage Learning, Boston, 2011.

[10] L. Mönch, Simulation-based benchmarking of production control schemes for complex manufacturing systems, Control Eng. Pract. 15 (2007) 1381-1393.

[11] P.J. Roache, Fundamentals of Verification and Validation, Hermosa Publishers, Socorro, NM, 2009.

[12] Instituto Brasileiro de Geografia e Estatística (IBGE), Censo Demográfico 2010: Dados referentes ao bairro Campo Lindo, Seropédica, RJ, 2010.

[13] W.O. Kermack, A.G. McKendrick, A contribution to the mathematical theory of epidemics, Proc. R. Soc. Lond. A 115 (1927) 700-721.

[14] Secretaria de Saúde, Informações sobre dengue: sintomas, prevenção e combate ao mosquito, https://www.saude.gov.br/dengue, 2024.

[15] R.A. Adams, J.J.F. Fournier, Sobolev Spaces, second ed., Academic Press, Amsterdam, 2003.

[16] L.A. Medeiros, M.M. Miranda, Espaços de Sobolev: iniciação aos problemas elípticos não homogêneos, Instituto de Matemática, UFRJ, Rio de Janeiro, 2019.

[17] H.M.S. Damian, M. Nascimento, Espaços de Sobolev em $\mathbb{R}^n$, 2019. Disponível em: https://www.ime.usp.br/ piccione/.

[18] C. Geuzaine, J.-F. Remacle, Gmsh: A 3-D finite element mesh generator with built-in pre- and post-processing facilities, Int. J. Numer. Methods Eng. 79 (2009) 1309-1331.

[19] NEAMP/PUCSP, Universidade Federal Rural do Rio de Janeiro (UFRRJ), 2023. Disponível em: https://neamp.pucsp.br/.

[20] ACCAMTAS, Degradação Ambiental em Seropédica, 2012. Disponível em: http://www.accamtas.com.br/.

[21] Instituto Nacional de Colonização e Reforma Agrária (INCRA), Página Oficial do INCRA, https://www.gov.br/incra/pt-br.

[22] INMET - Instituto Nacional de Meteorologia, Projeções Climáticas: Mapas de Precipitação e Temperatura Média Prevista para o Brasil, 2023.

[23] Brasil. Ministério da Saúde, Guia de vigilância em saúde: orientações sobre a prevenção e controle da dengue, 2024.

[24] J. Ahrens, B. Geveci, C. Law, ParaView: An end-user tool for large data visualization, in: Visualization Handbook, Elsevier, 2005.

[25] N.M. Ferguson, Modeling the impact of next-generation dengue vaccines in endemic settings, Nature Communications 16 (2025) 442.

[26] K. Salari, P. Knupp, Code Verification by the Method of Manufactured Solutions, Sandia National Laboratories, 2021.

[27] Y. Zhang, et al., Spatiotemporal modeling of vector-borne diseases in complex urban environments using high-resolution geographic data, Sci. Total Environ. 906 (2024) 167-182.

[28] M.U.G. Kraemer, et al., Global spatial dynamics of dengue: persistence, expansion and clinical impact, Science 387 (2025) 124-138.

This preprint was submitted under the following conditions:

- The authors declare that the necessary Terms of Free and Informed Consent of participants or patients in the research were obtained and are described in the manuscript, when applicable.
- The authors declare that the preparation of the manuscript followed the ethical norms of scientific communication.
- The authors declare that they are aware that they are solely responsible for the content of the preprint and that the deposit in SciELO Preprints does not mean any commitment on the part of SciELO, except its preservation and dissemination.
- The authors declare that the data, applications, and other content underlying the manuscript are referenced.
- The deposited manuscript is in PDF format.
- The authors declare that the research that originated the manuscript followed good ethical practices and that the necessary approvals from research ethics committees, when applicable, are described in the manuscript.
- The authors declare that once a manuscript is posted on the SciELO Preprints server, it can only be taken down on request to the SciELO Preprints server Editorial Secretariat, who will post a retraction notice in its place.
- The authors agree that the approved manuscript will be made available under a Creative Commons CC-BY license.
- The submitting author declares that the contributions of all authors and conflict of interest statement are included explicitly and in specific sections of the manuscript.
- The authors declare that the manuscript was not deposited and/or previously made available on another preprint server or published by a journal.
- If the manuscript is being reviewed or being prepared for publishing but not yet published by a journal, the authors declare that they have received authorization from the journal to make this deposit.
- The submitting author declares that all authors of the manuscript agree with the submission to SciELO Preprints.